First-in-human evaluation of cutaneous innate and adaptive immunomodulation by mosquito bites

David Guerrero[1,*], Hoa Thi My Vo[1,*], Chanthap Lon[3,*], Jennifer A. Bohl[2], Sreynik Nhik[3], Sophana Chea[3], Somnang Man[3,4], Sokunthea Sreng[3,4], Andrea R. Pacheco[3], Sokna Ly[3], Rathanak Sath[3], Sokchea Lay[1], Dorothee Missé[5], Rekol Huy[4], Rithea Leang[4], Hok Kry[6], Jesus G. Valenzuela[2], Fabiano Oliveira[2,$], Tineke Cantaert[1,$], Jessica E. Manning[2,3,$,#]

[1] Institut Pasteur du Cambodge, Pasteur Network, Phnom Penh, Cambodia

[2] Laboratory of Malaria and Vector Research, National Institute of Allergy and Infectious Diseases, National Institutes of Health, Rockville, Maryland, USA

[3] International Center of Excellence in Research, National Institute of Allergy and Infectious Diseases, National Institutes of Health, Phnom Penh, Cambodia

[4] National Center of Parasitology, Entomology, and Malaria Control, Phnom Penh, Cambodia

[5] MIVEGEC, Univ Montpellier, IRD, CNRS, 34000 Montpellier, France.

[6] Kampong Speu Provincial District, Ministry of Health, Phnom Penh, Cambodia

*co-first author

$ co-last author

corresponding author: jessica.manning@nih.gov

Abstract

Mosquito-borne viruses are a growing global threat. Initial viral inoculation occurs in the skin via the mosquito 'bite', eliciting immune responses that shape the establishment of infection and pathogenesis. To understand these phenomena, we assessed the cutaneous innate and adaptive immune responses via controlled *Aedes aegypti* feedings in humans living in an *Aedes*-endemic country. Gene expression profiling and immunophenotyping revealed induction of neutrophil degranulation and recruitment of skin-resident dendritic cells and M2-macrophages. As the immune reaction progressed over time, T cell priming and regulatory pathways were upregulated along with a shift to a Th2-driven response and CD8+ T cell activation. In accordance, participants' bitten skin cells produced less pro-inflammatory cytokines when stimulated by *Ae. aegypti* salivary gland extract. These results identify key immune genes, cell types, and pathways in the human response to mosquito bites that can be leveraged to develop novel therapeutics and vector-targeted vaccine candidates to arboviral diseases.

36 **Graphical Abstract**

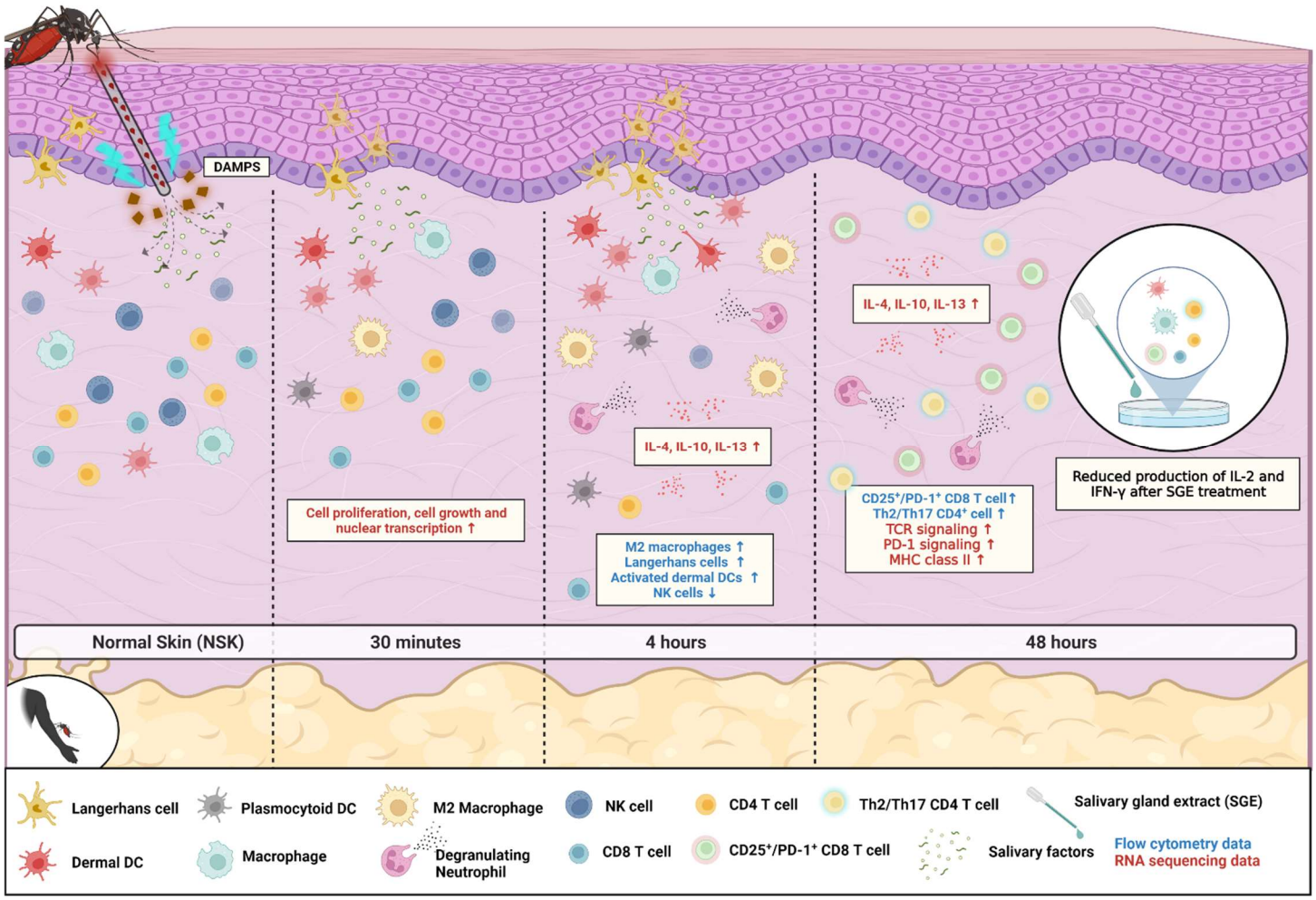

37

38

Introduction

With one million deaths every year, vector-borne diseases remain a major health problem worldwide[1]. In particular, arboviruses are of particular concern given a global distribution and a burden of nearly half a billion infections[2]. Several clinically significant arboviruses such as yellow fever (YFV), dengue (DENV), chikungunya (CHIKV), and Zika (ZIKV) viruses are all transmitted by *Aedes spp*. mosquitoes. These vectors are abundant in tropical and subtropical areas, but current climate change and rapid urbanization are expanding their transmission potential and increasing the at-risk population[3].

Mosquitoes first acquire an arbovirus via insertion of their proboscis into the dermis of an infected host during a blood meal. The virus then replicates in midgut cells to later disseminate and reach the salivary glands (SG)[4]. During a subsequent blood meal, the infectious mosquito inoculates virus and insect-derived molecules, including salivary components, into the dermis of a new human host. The saliva from hematophagous mosquitoes is a cocktail of pharmacologically active molecules, some of which are anti-hemostatic, angiogenic, and immunomodulatory[5–7]. Over the last couple decades, several animal and *in vitro* studies demonstrated that inoculation of vector saliva, and/or concomitant blood-feeding by an arthropod, can immunomodulate the host antiviral response in the skin and periphery[7–10]. These perturbations result in a dampening of the pro-inflammatory responses[11–13], promotion of recruitment of infection-susceptible cells to the bite site[14,15], stimulation of autophagy activation[5], and an induction of neutrophil infiltration to the local inflammation site[15] amongst other consequences. Mosquito-inoculated DENV or ZIKV infection in macaques led to higher or delayed viremia compared to non-vector or needle inoculation routes[16,17]. With regard to clinical pathogenesis, mice inoculated with both Semliki Forest virus and mosquito saliva had higher loads of virus RNA in the skin, earlier brain dissemination, and

62 more frequent lethal outcomes than animals inoculated with virus alone[12]. Taken together,
63 arthropod-mediated viral infection leads to increased disease progression, viremia, and
64 mortality[8,9]. Despite this robust evidence from animal and *in vitro* studies, there are no translational
65 studies on the human skin response to mosquito bites, much less those in tropical areas. Individuals
66 are continuously exposed to mosquito bites, possibly shaping their immune responses to mosquito
67 salivary proteins in contrast to those intermittently or rarely exposed[18,19]. In order to examine the
68 dermal and epidermal innate and adaptive immune responses to *Ae. aegypti* saliva, we compared
69 the immune responses before and after *Ae. aegypti* bites in skin biopsies from 30 healthy
70 Cambodian individuals living in an area where *Ae. Aegypti* mosquitoes are prevalent. Our study
71 provides information on the key genes and cell populations involved in the human immune
72 response at different time points after the 'mosquito bite.'

73 Results

74 Controlled *Aedes aegypti* bite challenge in healthy volunteers in Cambodia

75 From October 2020 to January 2021, we enrolled 30 healthy Cambodian adults at Kampong Speu
76 District Referral Hospital in Chbar Mon, Cambodia. The study population comprised 13 females
77 and 17 males, all of whom were of Khmer (Cambodian) ethnicity (Supplementary Table 1). The
78 population was randomly divided in three groups to assess immune responses by different
79 technologies (Fig. 1). The median age was 32.5 years (IQR 22–35) and the primary occupations
80 were variable, although nearly half (14/30) were unemployed. In terms of mosquito exposure risk,
81 most participants reported living in a house (20/30), being middle income (25/30), having one to
82 two domestic water containers (22/30). Notably, most participants did not use larvicide (28/30) or
83 insecticide (19/30) in their homes. Only 10% (3/30) reported prior dengue infection, but all 30
84 participants were positive for dengue anti-NS1 antibodies. All participants had detectable IgG to

85 *Ae. aegypti* salivary gland extract (SGE) prior to mosquito feeding, and these levels were not
86 significantly different by age, gender, or 14 days after the mosquito feeding (Extended Data Fig.
87 1). One participant did not complete Day 14 follow-up and was considered lost to follow-up. No
88 unanticipated adverse events occurred with the biopsies or mosquito feedings.

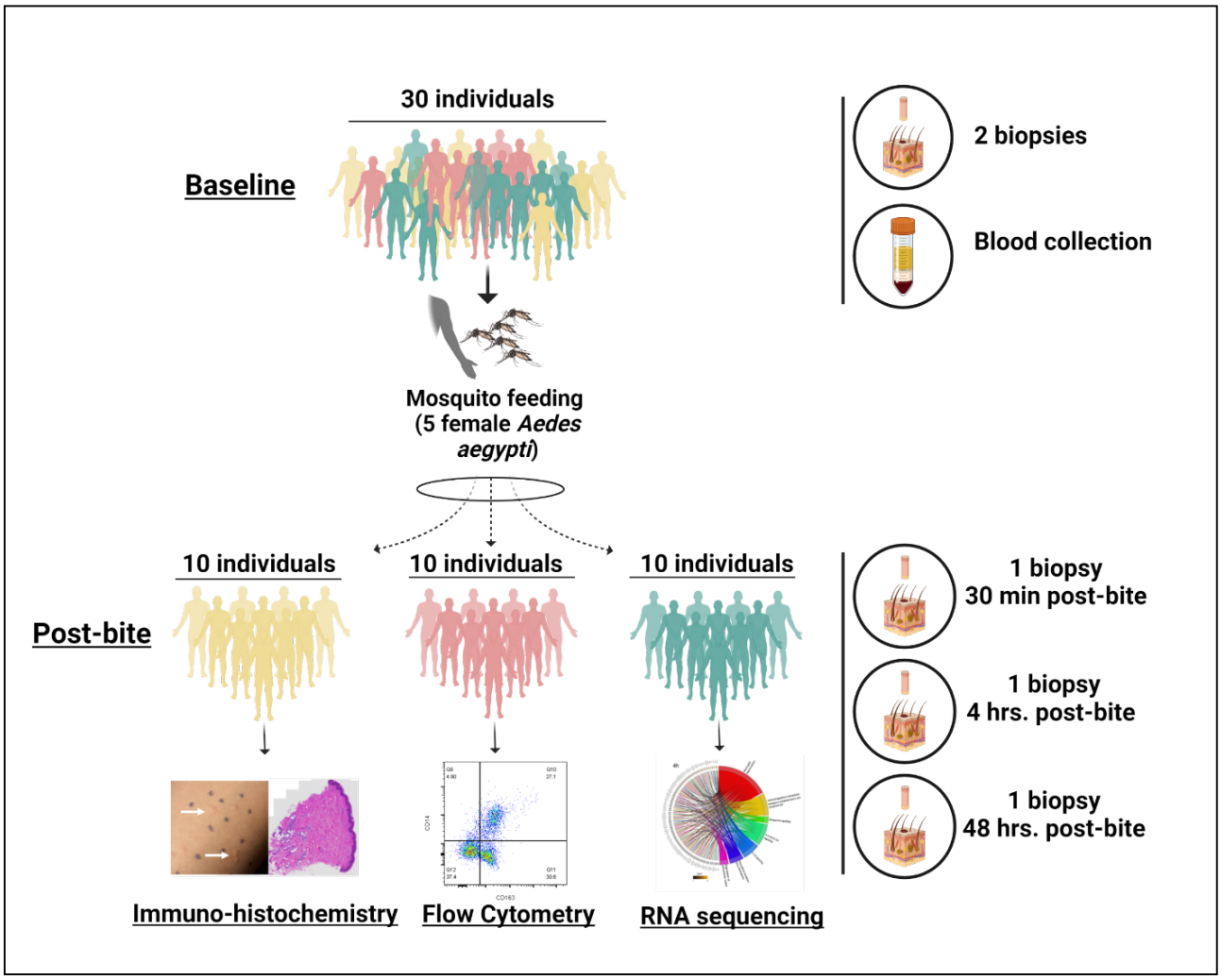

89

90 Figure 1. **Graphical Representation of Study Design.** Thirty Cambodian participants were
91 enrolled in the study. Each patient underwent a mosquito feeding (5 females *Aedes aegypti*) for
92 ten minutes. Each volunteer underwent a 3mm biopsy from the mosquito bite site at 30 minutes,
93 4 hours, and 48 hours. Additionally, two 3mm biopsies of normal skin (NSK) were taken from
94 the opposite forearm. Blood was collected to obtain serum.

Marked clinical changes occurred in the skin post-mosquito feeding

Exposure to five *Ae. aegypti* mosquitos resulted in 3 to 10 visible bite sites per volunteer. Upon clinical observation, participants experienced erythema and swelling with a "bite size" reaction that peaked at 15 minutes after feeding (Fig. 2a). The mean bite size of 4.9mm at 15 min after feeding decreased to 4.7 mm at 30 minutes, to 2.7 mm at 4 hours and gradually decreased to 2.1mm by 48 hours (Supplementary Table 1). Observation of representative histological sections shows increased recruitment of cells to the dermis and epidermis at 48 hours post-bite (Fig. 2b,c). There was no difference in bite size reaction by gender or age.

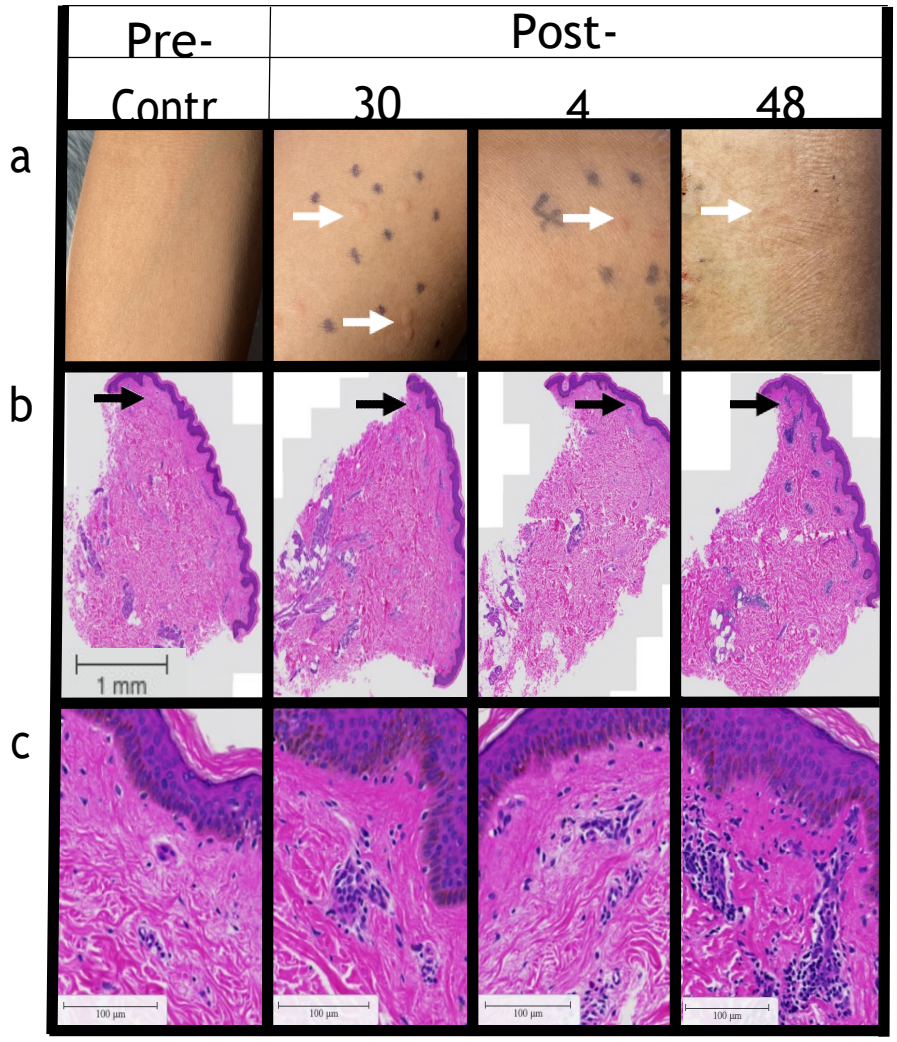

104 Figure 2. **Clinical observations of skin reaction pre- and post-bite on gross examination and**
105 **H&E staining. a,** Skin immune responses to mosquito bites (left to right) normal skin (NSK), 30
106 minutes, 4 hours, and 48 hours after exposure to five *Ae. aegypti* mosquitos. **b,** Representative
107 cross-sectional of 3mm punch biopsies H&E stained at (left to right) 0 hours, 30 minutes, 4 hours,
108 and 48 hours after exposure to *Ae. aegypti* bites. Scale bar is 1 mm. Black arrows indicate area of
109 infiltrate. **c,** Magnification of infiltrate indicated by black areas in B, scale bar 100μM.
110

111 **Changes in gene expression in *Aedes aegypti* bitten versus normal skin (NSK) evolved over**
112 **48 hours**

113 We extracted RNA and performed next generation sequencing on 40 skin biopsies from 10
114 participants (baseline normal skin (NSK) biopsy on the forearm, plus 3 follow-up biopsies each at
115 30 minutes, 4 hours, and 48 hours post *Ae. aegypti* bites on the contralateral arm). Principal
116 Component (PC) analysis of *Ae. aegypti* bite site skin biopsies resulted in segregation of sample
117 clusters based on the time the biopsy was taken (Fig. 3a), with PC1 and PC2 variances defining
118 differences between NSK and 30 minutes versus 4 hours and 48 hours. While PC3 variance
119 associated to the separation between biopsies taken at 4 hours and 48 hours, samples taken from
120 NSK (pink circles) and 30 minutes after *Ae. aegypti* bites clustered in the same spatial area. At 4
121 hours post-bite, 6 of 10 samples occupied a distinct region (Fig. 3a, blue ellipse) from NSK, 30
122 minutes or 48 hours after *Ae. aegypti* bites. Similarly at 48 hours post-bite, 7 of 10 samples
123 segregated into a discrete space (Fig. 3a, orange ellipse) compared to NSK, 30 minutes or 4 hours
124 after *Ae. aegypti* bites. These data indicate that time post-bite rather than inter-individual
125 differences drive unique patterns in gene expression. Differential analysis of RNA expression with
126 a threshold of two-fold ($-1 < \log2FC > 1$; False discovery rate (FDR) < 0.05) over NSK biopsies

127 resulted in 709 upregulated genes post-bite compared to 31 downregulated genes (Fig. 3b, red
128 circles). At 30 minutes, 4 hours, and 48 hours after a mosquito bite, 26, 210 and 473 genes were
129 upregulated over NSK, respectively (Fig. 3c, Supplementary Table 2). Conversely, one gene at 4
130 hours and 27 genes at 48 hours were downregulated after *Ae. aegypti* bites (Supplementary Table
131 2).

132 Upregulated genes at each time point were subjected to over-representation analysis (ORA) for
133 enriched pathways using the Reactome database with an FDR cut off < 0.05. Four pathways related
134 to cell proliferation, cell growth and nuclear transcription were identified (FDR < 0.05) at 30
135 minutes after *Ae. aegypti* bites (Supplementary Table 3). At both 4 and 48 hours post-bite, the
136 immune nature of the host response to *Ae. aegypti* bites was evident via the revealed pathways
137 (Fig. 3d, Supplementary Table 3). At 4 hours post-bite, pathways such as "neutrophil
138 degranulation", "Interleukin-4 and Interleukin-13 signaling", "Interleukin-10 signaling",
139 "Interferon-γ signaling" "Chemokine receptors bind chemokines" and "Immunoregulatory
140 interactions between a Lymphoid and a non-Lymphoid cell" (Fig. 3d, upper chord) were
141 significantly overrepresented and maintained until 48 hours post-bite (Fig. 3d, lower chord).
142 Unique pathways discovered at 4 hours post-bite were related to "degradation of extracellular
143 matrix" (Fig 3d, upper chord) while "antimicrobial peptides" pathway and "adaptive immune
144 system processes" were present at 48 hours post-bite including "TCR signaling", "Co-stimulation
145 by the CD28 family", "PD-1 signaling", "MHC class II antigen presentation" (Fig. 3d, lower
146 chord). A heatmap with differentially expressed genes (DEG) under an FDR cutoff < 0.05 and
147 log2FC >1 in at least one timepoint was assembled (Extended Data Fig. 3, Supplementary Table
148 4), showing the dynamics of DE expression throughout the three timepoints. Fig. 3e shows DEG
149 driving the common pathways found on Fig. 3d.

150 Overall, few DEG genes were detected at 30 minutes post-bite compared to NSK biopsies. The
151 main upregulated gene FOSB (up 18.8x) is one of the transcription factors of the FOS family
152 proteins that regulate cell proliferation and differentiation (Supplementary Table 2). As the
153 reaction progresses over time, gene expression increased towards neutrophil recruitment followed
154 by signaling of both Th1, Th2, and regulatory pathways. The five most regulated genes at 4 hours
155 compared to NSK are KRT6C (related to keratinization; up 80.8x), CXCL8 (neutrophil-attracting
156 chemokine IL-8 up 75.0x), TNIP3 (inhibitor of NF-kappa-B activation; up 59.3x), IL-20
157 (stimulates keratinocyte proliferation and differentiation; up 59.1x) and IL-1B (pro-inflammatory
158 cytokine; up 45.7x) (Supplementary Table 2). The immune response evolved at 48 hours post-bite
159 to include adaptive immune response pathways related to T-cell priming. The five top genes at 48
160 hours are KRT6C (related to keratinization; up 59.6x), DEFB4A (an antimicrobial peptide; up
161 32.7x), GZMB (Granzyme B, up 21.1x), TCL1A (proliferation of T and B cells; up 20.3x) and
162 CCL18 (chemokine associated with associated with TH2 responses; up 18.5x).

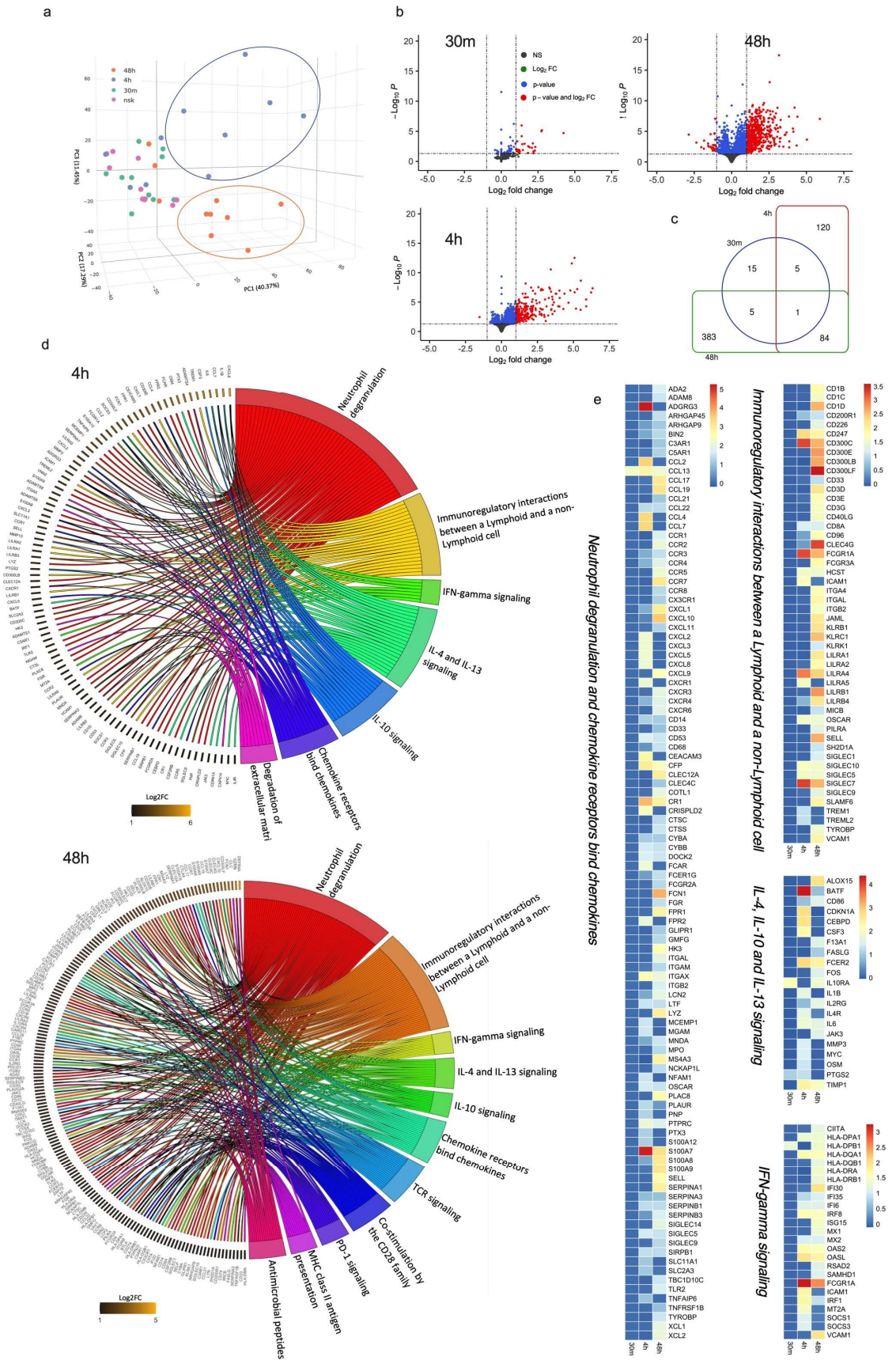
a
48h
4h
30m
nsk
PC1 (40.37%)
PC2 (17.29%)
PC3 (11.45%)
b
30m
48h
4h
NS
Log2 FC
p-value
p – value and log2 FC
Log2 fold change
c
4h
30m
48h
120
15
5
5
1
383
84
d
4h
48h
Neutrophil degranulation
Immunoregulatory interactions between a Lymphoid and a non-Lymphoid cell
IFN-gamma signaling
IL-4 and IL-13 signaling
IL-10 signaling
Chemokine receptors bind chemokines
Degradation of extracellular matri
TCR signaling
Co-stimulation by the CD28 family
PD-1 signaling
MHC class II antigen presentation
Antimicrobial peptides
Log2FC
e
Neutrophil degranulation and chemokine receptors bind chemokines
Immunoregulatory interactions between a Lymphoid and a non-Lymphoid cell
IL-4, IL-10 and IL-13 signaling
IFN-gamma signaling
30m
4h
48h

164 Figure 3. **Differential expression gene (DEG) and pathway analysis induced by *Aedesaegypti* mosquito bites over time. a,** 3D principal component analysis showing clustering of individual biopsies taken at 30 minutes (green dots), 4 hours (blue dots), 48 hours (orange dots) post-bite or normal skin (NSK; pink dots). Blue ellipse indicates clustering at 4 hours, while orange ellipse at 48 hours. **b,** Volcano plot comparing DEG from skin biopsies post-bite with NSK (significant genes with -1 < log2FC >1 and FDR < 0.05 are shown in red). **c,** Venn diagram summarizing the relationships between significantly upregulated genes over NSK (log2FC >1 and FDR < 0.05) and time post-bite. **d,** Chord plot shows significantly upregulated genes at 4 hours and 48 hours post-bite over NSK (left side of chord plot) and overrepresented pathways (right side of chord plot). Outer left ring shows genes and color range displays log2 fold change (left, key at bottom) or Reactome terms (outer right ring). Chords connect gene names with Reactome term pathways. **e,** Heatmap (scaled to log2FC) displaying a list of DEGs based on the common pathways overrepresented at 4- and 48-hours post-bite.

177

178 **Early innate immune response in the skin is characterized by increased proportions of DCs and M2 macrophages and a decreased proportion of NK cells**

180 To confirm and extend the gene expression analysis, dissociated cells from NSK and skin biopsies taken at 30 minutes and 4 hours after exposure to mosquitos, were characterized for innate and adaptive immune subsets by flow cytometry (Supplementary Table 5). No significant changes in cell populations were detected between NSK and 30 minutes post-bite, mirroring the transcriptomic analysis of DEG. At 4 hours post-bite, the proportion of dendritic cells (DC), and M2 macrophages increased, while the proportion of mast cells, natural killer (NK) and T-cells decreased, when compared to NSK and 30 minutes post-bite (Fig. 4a). The frequencies of DC

187 subsets and macrophages increased at 4 hours post-bite compared to NSK and 30 minutes (Fig. 4
188 b-h); a decreasing, though non-significant, trend in the NK cell population frequency was observed
189 over time (Fig. 4i). Within the DC subsets, Langerhans cells (CD45+CD3-CD207+) and activated
190 dermal DCs (CD45+CD3-CD1c+CD69+) increased at 4 hours compared to NSK while only
191 activated dermal DCs were increased at 30 minutes. (Fig. 4d, e). Regarding the macrophage
192 population, M2-skewed macrophages (CD45+CD14+CD163+) frequency increased after 4 hours
193 post-bite as well as their expression of activation markers (CD16/CD69) compared to NSK and 30
194 minutes (Fig. 4 f-h). Frequencies of activated M2 macrophages, activated dermal DCs, and
195 frequency of Langerhans cells positively correlated with clinically observed changes in bite size
196 at 30 minutes (Extended Data Fig. 2 a-c). The relative proportion of $CD4^+$ and $CD8^+$ T cells did
197 not change over time. Taken together, the results suggest that immune cell infiltration and
198 migration occurs in local skin tissue within 4 hours post-bite and is characterized by increased
199 frequencies of various DCs and M2 macrophages, but decreased frequencies of NK cells.

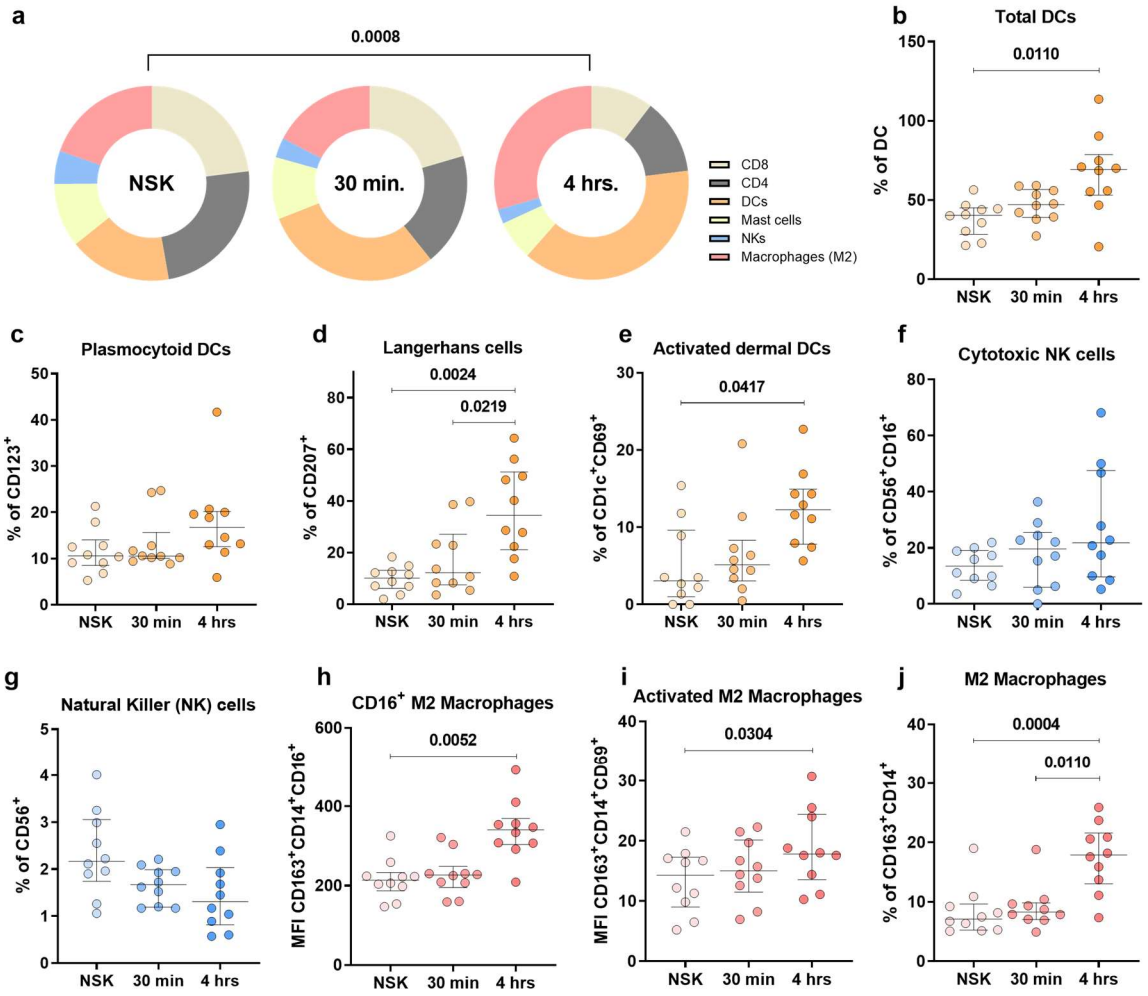

Figure 4. **Early innate immune responses in the skin are characterized by increased proportions of DCs and M2 macrophages, and a decreased proportion of NK cells at 4 hours post-bite**. **a,** Pie charts showing changes in the frequencies of skin immune cells during early innate immune response to mosquito bite at 30 minutes and 4 hours after exposure. **b-e,** Frequency changes in total DCs and subsets: Plasmacytoid DCs (CD123+), Langerhans cells (CD209+), and activated dermal DCs (CD1c+CD69+) at 4 hours post mosquito bites. **f-h,** Increase in M2 macrophages (CD14+CD163+) frequencies and their activation phenotypes (CD16+/CD69+). **i,** Frequency of NK cells (CD56+) in NSK, 30 minutes and 4 hours. **j,** Frequency of cytotoxic NK

209 cells in NSK, 30 minutes and 4 hours (CD56+CD16+). Statistical analysis were performed with
210 Chi-square test (**a**) and Friedman + Dunn's multiple comparisons test (**b-j**). Bars indicate median
211 and interquartile range.

212

213 **Changes in the T cell compartment are observable at 48 hours after mosquito 'bite'**

214 Changes in skin T cell populations were assessed using NSK and biopsies taken at 48 hours post-
215 bite. We found that the frequency of CD8+CD25+ and CD8+PD-1+ T-cells increased at 48 hours
216 post-bite, compared to the NSK (Fig. 5a). Frequencies of CD8+ T cells correlated inversely with
217 the bite size at 48 hours (Extended Data Fig. 2d). The frequency of effector memory cells re-
218 expressing CD45RA (T_{EMRA}) CD8 T cells (CD8+CCR7-CD45RA+) decreased at 48 hours (Fig.
219 5b). We observed a decrease in the frequency of Th1/Th17 (CD4+CCR4-CXCR3+) cells at 48h
220 compared to NSK and an increase in the frequency of Th2/Th17 (CD4+CCR4+CXCR3-) cells
221 (Fig. 5c). Within the CD4+ T cell compartment, the frequency of CD4+ effector memory T cells
222 (T_{EM}) (CD4+CCR7-CD45RA-) increased at 48 hours compared to NSK, while the frequency of
223 T_{EMRA} cells (CD4+CCR7-CD45RA+) decreased (Fig. 5c). Interestingly, no changes were
224 observed in the frequencies of skin-resident CD4 (CD4+CD103+CLA+) or CD8
225 (CD8+CD103+CLA+) T cells (Extended Data Fig. 4). At 48 hours post-bite, these results show
226 an increase in the frequency of activated/exhausted CD8 T cells in addition to a shift from
227 Th1/Th17 towards Th2/Th17 polarization of CD4 T cells.

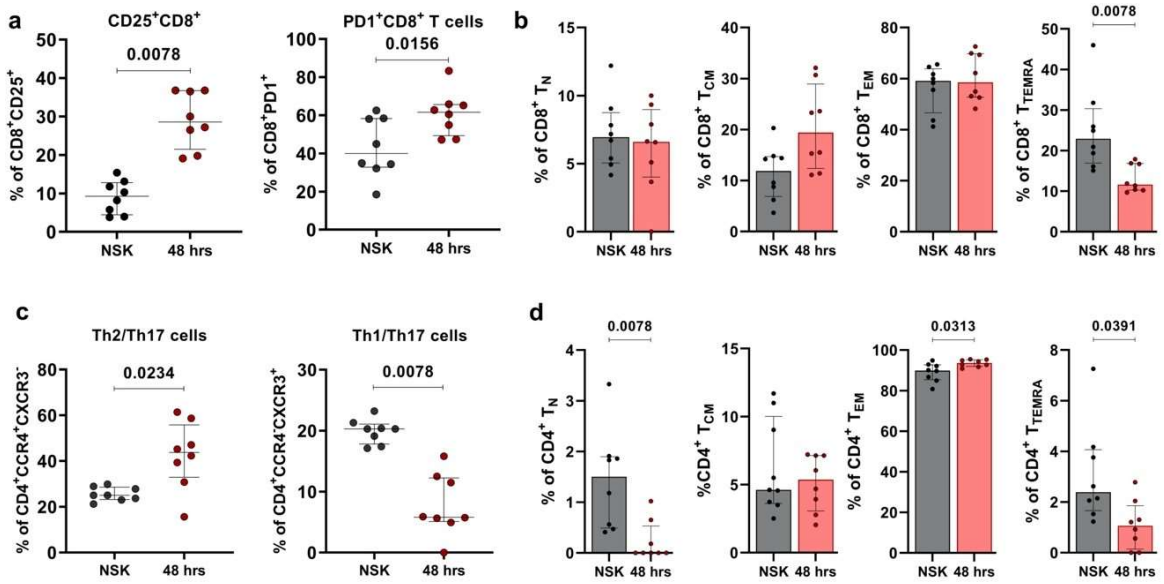

Figure 5. **Changes in the T cell compartment are observable at 48 hours after mosquito exposure. CD8 T cells exhibit a high activation/exhausted phenotype, while CD4 T effector memory cells decrease in their Th1Th17 compartment and increase their Th2Th17 compartment. a,** Increased frequency of CD25+ and PD1+ CD8 T cells at 48 hours post mosquito exposure. **b,** Frequencies of CD8 T cells naive (CCR7+CD45RA+), central memory (CCR7+CD45RA-), effector memory (CCR7-CD45RA-) and TEMRA (CCR7-CD54RA+) frequencies. **c,** decreased Th1/Th17 and increased Th2/Th17 effector memory CD4 T cell compartment at 48 hours. **d,** CD4 T cells naive (CCR7+CD45RA+), central memory (CCR7+CD45RA-), effector memory (CCR7-CD45RA-) and TEMRA (CCR7-CD54RA+) frequencies. Statistical analysis was performed with Wilcoxon signed-rank test. Bars indicate median and interquartile range.

241 **"Bitten" human skin cells stimulated by *Aedes aegypti* saliva produce significantly less pro-**
242 **inflammatory cytokines**

243 Next, we sought to assess if *Ae. aegypti* saliva impacted cytokine production by skin cells taken
244 48 hours post-bite. We measured pro- and anti-inflammatory cytokines released into the media
245 after a stimulation assay with and without *Ae. aegypti* SGE. We observed a significant reduction
246 in the levels of Interleukin 2 (IL-2) and Interferon gamma (IFN-γ) in the cells treated with both
247 SGE and PMA/Ionomycin compared to the cells treated with PMA/Ionomycin only (Fig. 6,
248 Extended Data Fig. 5). The levels of other pro-inflammatory cytokines like TNF-α, IL-17A and
249 IL-17F showed no significant change (Fig. 6). Similarly, no change in the regulatory cytokine IL-
250 10 was observed (Fig. 6). This data suggests that SGE has a dampening effect on the production
251 of pro-inflammatory cytokines IL-2 and IFN-γ under stimulatory conditions in "bitten" human
252 skin cells.

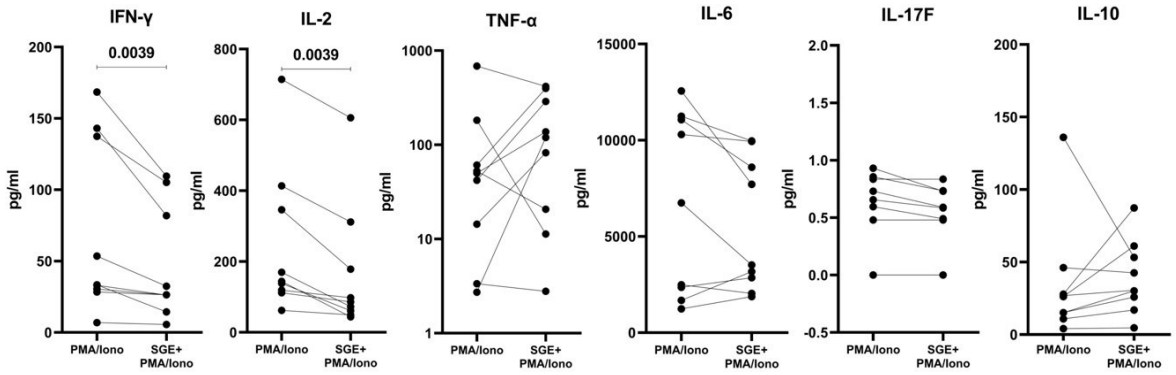

253

254 Figure 6. **Human skin cells obtained from *Ae. aegypti* bitten skin stimulated by *Ae. aegypti***
255 **salivary gland extract (SGE) produce significantly less pro-inflammatory cytokines (IL-2**
256 **and IFN-γ)**. Cytokine production measured in skin cell culture supernatant after treatment with

257 PMA/Ionomycin in the presence or absence of SGE. Statistical analysis was performed with
258 Wilcoxon signed-rank test.

259

260 **Discussion**

261 Arboviruses enter the host through the skin when the arthropod injects its saliva and other
262 components into the dermis while taking a bloodmeal. Data from mice and macaques suggest that
263 the unique dual presence of virus and saliva orchestrates an immunological cascade of events that
264 influence the establishment and course of infection[12,16,17]. To translate these findings to humans,
265 the current study assessed the dynamics of the cutaneous immune response to arthropod bites from
266 a clinically relevant vector, the *Ae. aegypti* mosquito, in humans from arboviral-endemic areas
267 with lifelong exposure to *Aedes* mosquitos. At 4 hours post-bite, we observed upregulation of
268 genes involved in neutrophil recruitment and increased frequencies of dendritic cells and M2
269 macrophages. As the immune response progressed over two days, we observed an increased
270 frequency of activated, PD-1^{+}CD8^{+} T cells, a polarization towards Th2/Th17 CD4^{+} T-cells, and
271 upregulation of IL-10, IL-4, and IL-13 and IFN-γ related pathways. Interestingly, these human
272 skin cells post-bite produced less pro-inflammatory cytokines when stimulated by *Ae. aegypti*
273 SGE.

274 A mosquito 'bite' results in minor tissue damage by the proboscis, injection of mosquito saliva
275 into the skin, and introduction of both mosquito and host microbiota into the skin. In this study,
276 we did not parse out the separate impact of each process on the skin immune response. Alterations
277 in skin immunity due to injury from the punch biopsy itself were mitigated by ensuring biopsy
278 sites were at least 10 to 20 mm away from one another and were not taken directly at the site of

279 the needle administration of subcutaneous lidocaine. The effect of local anesthetic was mitigated
280 by the case-control design that each person's anesthetized, bitten skin was compared to
281 anesthetized, unbitten skin, presumably negating any immediate cutaneous immune effects
282 attributed to lidocaine, for which the literature is sparse.

283 Mosquito bites cause a local cutaneous reaction with wheal and flare manifestation[20,21].
284 Concordantly, the bite size reaction peaked after 15 minutes post-bite in this endemic study
285 population. Few changes were detected in gene expression or influx and activation of innate
286 immune cells at the 30 minutes post-bite time point. Upregulated genes were related to top-level
287 processes such as signal transduction. We did not design this study to assess the role of pre-stored
288 immune mediators such as histamine (and others) in the development of edema and their
289 modulation in the immune response. Indeed, mosquito bites can activate cutaneous mast cells,
290 which are prominent histamine-storing cells, and induce their degranulation. The release of
291 histamine and other mediators leads to vasodilation, fluid accumulation at the bite site, and
292 neutrophil influx, which were all ultimately observed here[20,21].

293 As the immune reaction progressed, the mosquito 'bite' induced degradation of the extracellular
294 matrix (ECM), and a strong influx of leukocytes at 4 hours post-bite, consistent with previous
295 animal observations[22]. We observed several disintegrin and metalloprotease with thrombospondin
296 type I motifs (ADAMTS) were upregulated, mostly at 4 hours post-bite, that can be associated
297 with ECM degradation. Similarly, granzyme B (GZMB) upregulated at 48 hours, despite its effects
298 on inducing inflammation it may also be involved in ECM degradation using as substrate
299 fibronectin, vitronectin, laminin and others[23,24]. Saliva from blood-feeding arthropods contains
300 anti-hemostatic proteins that prevent coagulation and promote vasodilation, leading to increased
301 leukocyte trafficking[20,25]. These processes – extracellular matrix degradation and vasodilation –

302 can facilitate viral infection by disrupting vascular functions, as is the case of sialokinin, a
303 mosquito salivary protein that hinders endothelial barrier integrity[26]. In addition, elevated
304 leukocyte trafficking can facilitate viral replication by augmenting the proportion of susceptible
305 cells to the local inoculation site[12,15,26]. Indeed, as most leukocyte subsets are permissive to
306 infection by most arboviruses, they play a dual role in the infection process: both as replication
307 targets/dissemination vehicles and as the first line of defense.

308 The strong influx of activated M2 macrophages, DCs and Langerhans cells at 4 hours post-bite
309 highlight the cellular trafficking role initiated by 'the bite' that can ultimately result in viral
310 dissemination. Upregulated chemokines such as CCL2 and CCL7, attracting mainly monocytes,
311 DCs and T cell, may be participating in this recruitment[27]. M2-polarized macrophages produce
312 anti-inflammatory cytokines, mediate wound healing processes, and support Th2 responses [28].
313 Moreover, activation of dermal DCs and M2 macrophages positively correlated with the bite size
314 in our study. Upon stimulation, DCs upregulated CD69, preventing them from exiting the tissue
315 and improving the likelihood of antigen internalization. Subsequent CD69 downregulation
316 promotes Sphingosine-1-Phosphate (S1P1) leading to DC migration to the lymph nodes[29]. The
317 CD69-S1P1 mechanism of cell retention in tissue is also well-described for resident T cells,[30]
318 whose role in saliva-mediated immunity is not yet known.

319 *Ae. aegypti* mosquito saliva has a clear impact on neutrophil influx and degranulation. Two
320 recently identified *Ae. aegypti* salivary proteins (NeSt1 and AgBr1) that attract and stimulate
321 neutrophils at the 'bite site,' changing the immune microenvironment and leading to increased
322 early ZIKV replication and enhanced pathogenesis[14,15]. Here, at 4 hours post-bite, chemokines
323 CXCL2, CXCL3, CXCL5, and especially CXCL8, plus the cytokine IL-1B were upregulated
324 returning to levels comparable to NSK at 48 hours post-bite. CXCL2-5 chemokines are responsible

325 for attracting neutrophils and exhibiting angiogenic properties[31]. Pro-inflammatory responses
326 through inflammasome activation and IL-1B production can trigger a sustained neutrophilic
327 response.[32] Microbiota egested during infected sand fly bites contributed to IL-1B production[33].
328 On the other hand, IL-20 was upregulated at 4 hours post-bite. IL-20 is most active at epithelial
329 sites downregulating IL-1B resulting in deactivation of neutrophil functions such as phagocytosis,
330 granule exocytosis, and migration[34,35]. Increased gene expression for neutrophil recruitment and
331 degranulation at 4 hours post-bite in our Cambodian study population further supports the timing
332 of neutrophil influx seen 3 hours post-bite in bite-experienced C57BL/6 immunocompetent mice[12].
333 How the timing of neutrophil influx would differ in a bite-naïve population is a question that
334 remains to be answered.

335 As the immune response transitioned from innate to adaptive, a strong T-cell signature emerged at
336 4 and 48 hours emerged after the mosquito 'bite'. CD8+ T cell activation was confirmed by
337 increased expression of CD25, an early activation marker. Skin CD8+ T cells also upregulate PD-
338 1 expression, an immune-checkpoint receptor that is induced by yet can also inhibit T cell
339 activation. PD-1 primarily inhibits effector function acquisition by T cells, the loss of sensitivity
340 after T cell receptor signaling and modulation of cytotoxicity, and inhibition of TNF-α and IL-2
341 production along with T-cell expansion[36,37]. Interestingly, highly activated CD8+ cells have been
342 observed in skin from dengue shock syndrome patients[38]. Here at 4 and 48 hours post-bite, CD4+
343 T cells had a skewed phenotype to Th2-like cells and IL-10, IL-13, and IL-4 related pathways were
344 upregulated compared to NSK. CCL18, upregulated at 48 hours post-bite, can be expressed by M2
345 macrophages and is linked to increased IL-4, IL-10, and IL-13, especially in the presence of
346 histamine[39]. Indeed, initial animal experiments also pointed to a Th2-mediated allergic
347 inflammatory response following mosquito bites or inoculation with SGE[13].

348 At 48 hours post-bite, other upregulated genes such as CD28, ICOS, and CTLA-4 suggest a
349 regulatory role of the CD4+ compartment in controlling the local immune responses to *Ae. aegypti*
350 saliva. Th2 polarization is essential to avoid excessive collateral damage from an exacerbated pro-
351 inflammatory response, especially in a situation where the skin immune cells are repeatedly
352 exposed to the same type of insult, as is the case with individuals living in tropical areas of
353 mosquito abundance. Blood DC antigen-2 (CLEC4C), upregulated at 48h compared to NSK, is
354 thought to signal through BDCA-2 to inhibit activation of the NF-κB pathway, inhibit production
355 of type I IFNs, and block TRAIL-mediated cytotoxic activity[40]. This may represent a possible
356 mechanism that differentiates chronically exposed individuals compared to naïve individuals.

357 To consider other potential mechanisms that immunomodulate the microenvironment, we noted
358 increased expression at 48 hours post-bite of ficolin-1 (FCN1), a complement lectin pathway
359 protein that may bind and opsonize mosquito microbiota or salivary components, then activate the
360 complement pathway[41]. Another C-type lectin receptor LSECtin (CLEC4G, increased at 48 hours
361 compared to NSK) negatively regulates T cell-mediated immunity and may be also linked to
362 apoptotic cell clearance by macrophages[42]. Of note, the upregulation of CXCL10 chemokine and
363 its receptor CXCR3 are linked to their major roles of inflammatory reactions, T cell migration, and
364 IFN-γ in the saliva-mediated process[43]. Besides chemokines, the top expressed molecule was an
365 antimicrobial peptide hBD-2 (DEFB4A), produced by neutrophils and keratinocytes. DEFB4A is
366 a marker of inflammation absent in normal skin and responsible for recruitment of memory T cells,
367 immature DCs, mast cells and neutrophils[44,45].

368 In this study, the presence of mosquito saliva inhibited pro-inflammatory cytokine production by
369 'bitten' human skin cells after *in vitro* re-stimulation with saliva. This cytokine-dampening effect
370 may partly result from the interaction between salivary components and key checkpoints on

371 different signaling pathways. One example includes the salivary protein LTRIN known to interfere
372 with the Nf-kB pathway by binding to LTβR, thus hindering its dimerization and leading to
373 decreased production of inflammatory cytokines[11]. On the other hand, skin immune tolerance to
374 constant mosquito exposure may also explain the reducing effect of SGE on cytokine production
375 as seen here in our bite-experienced participants[12,19,46].

376 With the current rise of vector-borne diseases around the world, future clinical development of
377 vector-targeted strategies for both known and unknown vector-borne diseases will require a
378 fundamental understanding of how vector saliva modulates the cutaneous immune response of
379 humans. Translational studies, such as the one presented here, significantly expand our current
380 knowledge on human skin immunity and the immune response orchestrated by a 'mosquito bite'.
381 These newly identified genes, cell types, and processes of human cutaneous immunity can be
382 leveraged in the development of novel therapeutics and vector-targeted vaccine candidates. Such
383 new pathogen-agnostic strategies have shown promising results in recent years from vector saliva-
384 based vaccinations to topical antiviral applications post-bite [47–50]. To build the next generation of
385 countermeasures against vector-borne disease, nuanced and comprehensive understanding ofskin
386 immunity to both pathogen and vector saliva alike will be required.

387

388 Materials and methods

389 Study Enrollment and Procedures

390 From October 2020 to January 2021, we enrolled thirty Cambodian adults at Kampong Speu
391 District Referral Hospital. Eligible participants were healthy adults between the ages of 18 and 45
392 years old who agreed not to use topical or oral antihistamines or steroids for the duration of the

393 study. Participants were excluded if they were pregnant or reported a history of severe allergic
394 reaction to mosquito or other insect bites, use of medications that affect blood clotting, or history
395 of significant scarring such as keloid formation (full criteria found on
396 https://clinicaltrials.gov/ct2/show/NCT04350905). All participants provided written informed
397 consent before enrollment, and the study was conducted in accordance with the provisions of the
398 Declaration of Helsinki and Good Clinical Practice guidelines.
399 On Day 0, five starved uninfected *Ae. aegypti* female mosquitos were selected from a mosquito
400 colony dedicated to human feeding studies in the Malaria and Vector Research Laboratory at the
401 National Center for Parasitology, Entomology and Malaria Control. Mosquitos fed through the
402 disposable mesh of a feeding device placed on participants' ventral forearm skin for 10 minutes.
403 Redness and swelling in millimeters were assessed immediately, 15 minutes, 30 minutes, 4 hours
404 and 48 hours after feeding. Redness and swelling were measured in millimeters at 15 minutes, 30
405 minutes, and 4 hours.

406 A total of five 3-mm skin punch biopsies were performed on each individual: one biopsy from
407 bitten skin per time point (30 minutes, 4 hours, and about 48 hours after feeding is completed) for
408 a total of three 'bitten' biopsies, and two from NSK collected at baseline. Less than 1cc of 0. 2%
409 lidocaine without epinephrine was delivered via 30-G needle each chosen 'bite' at the time of
410 biopsy and 3-mm biopsy was performed on 'bite' adjacent to needle puncture. For feasibility of
411 skin sample analysis, each participant was assigned to 1 of 3 technical modality cohorts: 1)
412 immunohistochemistry, 2) RNASeq, and 3) flow cytometry with ten people in each cohort.
413 Additionally, blood was collected for serological and cellular analyses at baseline and 14 days
414 after feeding.

415 ***Aedes aegypti* salivary IgG enzyme-linked immunosorbent assays**

416 *Ae. aegypti* SGE (prepared from homogenized, dissected salivary glands) was diluted to a concentration of
417 2 ug/ul in carbonate-bicarbonate buffer (Millipore-Sigma) and used to coat 96-well Immulon 4x HB plates
418 (Nunc) overnight at 4°C. Plates were blocked in a solution of TBS 4 % Bovine serum albumin 0.025 %
419 Tween 20 (Millipore-Sigma). Each plate included sera in duplicate (1:200 dilution in blocking solution)
420 from all time points, a negative control (non-reactive human sera to SGE), an internal control (a pool of
421 positive sera to SGE with optical density (OD) set to 0.25 at 450nm) and blank wells. Secondary antibody
422 [goat anti-human IgG alkaline phosphatase (1:10000 in blocking solution; Millipore-Sigma). A solution of
423 p-nitrophenylphosphate (Millipore-Sigma) was used as substrate and OD measured at 450nm in arbitrary
424 enzyme-linked immunosorbent assay (ELISA) units.

425 **Dengue IgG enzyme-linked immunosorbent assays**

426 The PanBio® Dengue Indirect IgG ELISA (product code 01PE30) was performed according to
427 the manufacturer's instructions. Two microtiter plates were supplied, one containing stabilized
428 dengue-1 through dengue-4 (antigen plate) and the other containing either anti-human IgM or anti-
429 human IgG bound to separate wells (assay plate). Peroxidase-labeled anti-dengue virus
430 monoclonal antibody (125 µl/well) was added to the antigen plate to solubilize the antigens and
431 form antibody-antigen complexes. Concurrently, 100 µl of patient serum was diluted 1:100 in the
432 provided diluent and added to each well of the assay plate containing either bound anti-human IgM
433 or bound anti-human IgG, and human IgM or IgG in the patient's serum was captured. The plates
434 were incubated for 1 h at room temperature (antigen plate) or 37°C (assay plate); then the assay
435 plate was washed, and 100 µl of antibody-antigen complexes per well was transferred from the
436 antigen plate to the assay plate. These complexes were captured by dengue virus-specific IgM or
437 IgG during incubation for 1 h at 37°C. The plate was washed, and bound complexes were
438 visualized through the addition of 100 µl of tetramethylbenzidine substrate per well. After 10 min,
439 the reaction was stopped by the addition of 100 µl of 1 M phosphoric acid per well, and the strips

440 were read at 450 nm with a microtiter plate reader. Positivity was determined by comparison to
441 the IgM and IgG reference sera provided (cutoff calibrators). A positive sample was defined as
442 having a sample/calibrator absorbance ratio of ≥1.0, and a negative sample was defined as having
443 a ratio of <1.0.

444 **Formalin preservation and H&E staining of skin biopsies**

445 Biopsies were placed in 7ml prefilled 10% formalin vials (Azer Scientific) and stored at 4°C until
446 paraffin embedded. Unstained slides were cut from paraffin blocks and deparaffinized in xylene,
447 then hydrated through graded alcohols up to water, placed in Carazzi's hematoxylin, washed in
448 tap water, and put in one change 95% ethanol. Next, they were placed in eosin-phloxine solution
449 and then run through graded alcohols to xylene. After xylene, the stained slides were than a cover
450 slip was mounted using Permount Mounting Media (Fisher Scientific).

451 **RNA extraction, RNA-seq library preparation, sequencing and analysis.**

452 Biopsies were stored in DNA/RNA Shield (Zymo research) and kept in 4 °C until processing. Skin
453 was homogenized using 3mm zirconium beads (Biolink laboratories) and a Magnalyser bead
454 beater (Roche Diagnostics®). After homogenization total RNA was loaded at InnuPure® C16
455 touch (AnalitikJena) for magnetic separation of total RNA using an InnuPREP® RNA Kit–IPC16
456 (AnalitikJena). Quality of extractions was verified on a 4200 TapeStation (Agilent) and all samples
457 had RIN numbers above seven. RNA sequencing was performed by Novogene. Briefly, mRNA
458 was enriched by Poly (A) capture and RNA libraries were prepared using the NEBNext Ultra II
459 Directional RNA Library Prep Kit for Illumina (New England Biolabs) and sequenced on a
460 NovaSeq 6000 (Illumina) generating paired end reads at 150 bp length. After removing low quality
461 reads (Trimommatic 0.39)[51], mapping to the human genome (hg38; GCF_000001405.39) and
462 gene-level quantification were generated by RSEM 1.3.2[52], Bowtie 2-2.4.2[53] and SAMtools

463 1.11[54]. Normalization and differential gene expression (DGE) analysis were performed using
464 DESeq2 1.34.0[55], employing the variance stabilizing transformed function (VSN 3.62.0)[56] to the
465 count matrix, that was designed to account for paired samples enabling expression analyses with
466 normal skin samples from the same subject as reference. Approximate Posterior Estimation for
467 GLM (Apeglm 1.16.0) method was used to calculate fold change of DEGs[57]. DEGs were
468 considered significant if apeglm-estimated shrunken log2fold change was <1 or >1 and with a false
469 discovery rate <0.05 (Benjamini–Hochberg multiple testing correction method[58]). PlotPCA3D
470 0.0.1(twbattaglia/btools) was used to generate tri-dimensional principal component analysis plots
471 on DESeq2. EnhancedVolcano 1.12.0 was used to generate volcano plots[59]. GOplot 1.0.[60] was
472 used to generate chord plots using data obtained from packages clusterProfiler 4.2.0[61] and
473 ReactomePA 1.38.0[62]. Pathways with a Benjamini–Hochberg corrected P value <0.05 and were
474 considered as enriched, selected pathways were mapped on chord plots[58]. Heatmaps were prepared
475 using package pheatmap 1.0.12.[63] and dendsort 0.3.4[64]. All DEG analyses were performed using
476 R 4.1.0[65].
477
478 **Skin biopsy dissociation**
479 Biopsies were transported in RPMI media (Sigma-Aldrich) at 4 °C. Whole skin dissociation kit
480 (Miltenyi®) was used to perform the biopsies dissociation. An enzyme mix consisting of enzyme
481 D, enzyme A and buffer L was prepared according to the manufacturer's specifications. Single
482 punch biopsies were incubated in 400 µl of dissociation mix, at 37°C – 5% CO2 overnight.
483 Following incubation, each sample mix was transferred to a Falcon round-bottom tube with cell-
484 strainer cap (40-75um). Using a rubber pestle and the cell-strainer cap as a mortar, biopsies where
485 gently macerated to increase cell recovery yield. 500 µl of cold RMPI was used to rinse caps.

486 Samples were then centrifuged at 1500 rpm 4°C for 10 minutes and the pellet resuspended in 500
487 µl of cold RPMI. Dissociated skin cells were counted using a pre-programmed setting in a
488 Countess™ II FL Automated Cell Counter.

489 **Flow cytometry**

490 Dissociated cells were seeded on round bottom 96-well plates and washed with 200 µl of
491 ThermoFisher's PBS buffer 1x (1500 rpm, 4°C for 5 minutes). Twenty µl of Biolegend Zombie
492 Aqua fixable viability stain (1:500) was added and incubated for 20 minutes in the dark at 4°C.
493 Excess viability stain was washed away with 200 µl of PBS/BSA/EDTA buffer (1500 rpm, 4°C
494 for 5 minutes), and the pellet resuspended and incubated for 10 minutes at 4°C in 4 µl of
495 Biolegend's FcR blocking antibody (1:10). Cells were then incubated for 30 minutes at 4°C with
496 surface staining antibody master mix. After washing free unbound antibody with 200 µl of PBS
497 (1500 rpm, 4°C for 5 minutes), cells were fixed with 100 µl of Biolegend's fixation buffer 1x for
498 20 minutes at 4°C in the dark. Following fixation, cells were permeabilized and washed with 100
499 µl of Biolegend perm-wash solution 1x (1500 rpm, 4°C for 5 minutes) and the pellet resuspended
500 and incubated for 30 minutes at 4°C in intracellular staining antibody master mix. Stained cells
501 were placed in 200 µl of PBS/BSA/EDTA 1x and visualized on a BD Biosciences FACS Aria II
502 using FACS Diva software. Analysis was performed using BD Biosciences FlowJo software.
503 Antibody panels are described in supplemental material (Supplementary Table 5).

504 **Multiplex cytokine screening**

505 The supernatants were collected from 24-hour stimulation cultures of dissociated skin cells and
506 stored at -20°C. Cytokines in the cell culture supernatants were quantified using Human Th
507 Cytokine Panel (12-plex) (Cat. 741027, BioLegend) according to the manufacturer's instructions.

508 All samples in the experiment were measured in duplicate. Briefly, undiluted supernatants were
509 incubated with beads coated with capture antibodies specific for IL-2, 4, 5, 6, 9, 10, 13, 17A, 17F,
510 22, IFN-γ and TNF-α for 2 hours at room temperature on shaker. After incubation, beads were
511 washed and incubated with biotin-labeled detection antibodies for 1 hour, followed by a final
512 incubation with streptavidin-PE for 30 minutes at room temperature on shaker. Beads were washed
513 and re-suspended with washing buffer. Beads were analyzed by flow cytometry using a FACS
514 Canto cytometer. Analysis was performed using the LEGENDplex analysis software v8.0, which
515 distinguishes between the 12 different analytes on basis of bead size and internal dye.

516 **Statistical analyses**

517 Flow cytometry and multiplex cytokine screening data were analyzed using the non-parametric-
518 based tests, Wilcoxon signed-rank and Chi-square test. Correlation analysis was performed with
519 the Pearson's correlation coefficient. Bars indicate median and interquartile range, and p-values
520 *$p<0.05$, **$p<0.01$, ***$p<0.001$. Statistical analysis of RNAseq data is described above.

521 **Acknowledgements**

522 We would like to thank the study participants in Kampong Speu, Cambodia. We would also like
523 to acknowledge Noemi Kedei and Maria Hernandez for their assistance in histology and staining.

524 **Funding**

525 This work was funded by the Division of Intramural Research at National Institute of Allergy and
526 Infectious Diseases at the National Institutes of Health. T.C. is a HHMI-Wellcome international
527 research scholar (208710/Z/17/Z). D.M is funded by the French National Research Agency (ANR-
528 **17**-CE15-00029) . D.G. is supported by a Calmette-Yersin PhD scholarship funded by the Institute
529 Pasteur International Network.

Competing interests

The authors declare no competing interests.

Author contributions

Conceptualization: F.O., J.E.M., T.C., J.G.V. Methodology: D.G., H.V, S.N., S.C., J.A.B., F.O., J.E.M.. Investigation: D.G., H.V, J.A.B, S.N., S.C., A.P., J.G.V., F.O., J.E.M. Visualization: D.G., F.O., J.A.B. Funding acquisition: F.O., J.E.M. Study enrollment and clinical procedures: C.L, S.L., R.S, S.S., S.N., J.M, H.K, R.L. Project administration: C.L., T.C., F.O., J.E.M., Supervision: T.C., D.M, F.O., J.E.M., C.L, R.L., H.R, H.K. Writing original draft: D.G., H.V., T.C., F.O., J.E.M., J.A.B. Writing review and editing: T.C., D.M., C.L., F.O., J.A.B., J.E.M.

All authors contributed to the article and approved the submitted version

Data availability

The Illumina raw reads (fastq files) were loaded at the NCBI Sequence Read Archive with accession numbers SRR18215008 to SRR18215047 and deposited in GenBank under bioproject accession code PRJNA812009. All data generated or analyzed during this study are included in this published article (and its supplementary information files). Clinical trial data is available at https://clinicaltrials.gov/ct2/show/NCT04350905. Flow cytometry data can be made available upon reasonable request directly to the authors.

Bibliography

1. WHO. A global brief on vector-borne diseases. *www.who.int* (2020).
2. Pierson, T. C. & Diamond, M. S. The continued threat of emerging flaviviruses. *Nat. Microbiol.* **5**, 796–812 (2020).

551 3. Ryan, S. J., Carlson, C. J., Mordecai, E. A. & Johnson, L. R. Global expansion and
552 redistribution of Aedes-borne virus transmission risk with climate change. *PLoS Negl. Trop.*
553 *Dis.* **13**, e0007213 (2019).
554 4. Godoy, R. S. M. *et al.* Dengue and Zika virus infection patterns vary among Aedes aegypti
555 field populations from Belo Horizonte, a Brazilian endemic city. *PLoS Negl. Trop. Dis.* **15**,
556 e0009839 (2021).
557 5. Sun, P. *et al.* A mosquito salivary protein promotes flavivirus transmission by activation of
558 autophagy. *Nat. Commun.* **11**, 260 (2020).
559 6. Ha, Y.-R. *et al.* Detection of Heparin in the Salivary Gland and Midgut of Aedes togoi.
560 *Korean J. Parasitol.* **52**, 183–188 (2014).
561 7. Schneider, B. S. & Higgs, S. The enhancement of arbovirus transmission and disease by
562 mosquito saliva is associated with modulation of the host immune response. *Trans. R. Soc.*
563 *Trop. Med. Hyg.* **102**, 400–408 (2008).
564 8. Guerrero, D., Cantaert, T. & Missé, D. Aedes Mosquito Salivary Components and Their
565 Effect on the Immune Response to Arboviruses. *Front. Cell. Infect. Microbiol.* **10**, 407
566 (2020).
567 9. Manning, J. E. & Cantaert, T. Time to Micromanage the Pathogen-Host-Vector Interface:
568 Considerations for Vaccine Development. *Vaccines* **7**, 10 (2019).
569 10. Vogt, M. B. *et al.* Mosquito saliva alone has profound effects on the human immune system.
570 *PLoS Negl. Trop. Dis.* **12**, e0006439 (2018).
571 11. Jin, L. *et al.* Salivary factor LTRIN from Aedes aegypti facilitates the transmission of Zika
572 virus by interfering with the lymphotoxin-β receptor. *Nat. Immunol.* **19**, 342–353 (2018).

573 12. Pingen, M. *et al.* Host Inflammatory Response to Mosquito Bites Enhances the Severity of
574 Arbovirus Infection. *Immunity* **44**, 1455–1469 (2016).
575 13. Schneider, B. S., Soong, L., Zeidner, N. S. & Higgs, S. Aedes aegypti salivary gland extracts
576 modulate anti-viral and TH1/TH2 cytokine responses to sindbis virus infection. *Viral*
577 *Immunol.* **17**, 565–573 (2004).
578 14. Hastings, A. K. *et al.* Aedes aegypti NeSt1 Protein Enhances Zika Virus Pathogenesis by
579 Activating Neutrophils. *J. Virol.* **93**, e00395-19, /jvi/93/13/JVI.00395-19.atom (2019).
580 15. Uraki, R. *et al.* Aedes aegypti AgBR1 antibodies modulate early Zika virus infection of
581 mice. *Nat. Microbiol.* **4**, 948–955 (2019).
582 16. McCracken, M. K. *et al.* Route of inoculation and mosquito vector exposure modulate
583 dengue virus replication kinetics and immune responses in rhesus macaques. *PLoS Negl.*
584 *Trop. Dis.* **14**, e0008191 (2020).
585 17. Dudley, D. M. *et al.* Infection via mosquito bite alters Zika virus tissue tropism and
586 replication kinetics in rhesus macaques. *Nat. Commun.* **8**, 2096 (2017).
587 18. Trager, W. Acquired Immunity to Ticks. *J. Parasitol.* **25**, 57(1939).
588 19. Guilbride, D. L., Guilbride, P. D. L. & Gawlinski, P. Malaria's deadly secret: a skin stage.
589 *Trends Parasitol.* **28**, 142–150 (2012).
590 20. Conway, M. J. Type I hypersensitivity promotes Aedes aegypti blood feeding. *Sci. Rep.* **11**,
591 14891 (2021).
592 21. Demeure, C. E. *et al.* Anopheles Mosquito Bites Activate Cutaneous Mast Cells Leading to a
593 Local Inflammatory Response and Lymph Node Hyperplasia. *J. Immunol.* **174**, 3932–3940
594 (2005).

595 22. Conway, M. J. *et al.* Mosquito Saliva Serine Protease Enhances Dissemination of Dengue
596 Virus into the Mammalian Host. *J. Virol.* **88**, 164–175 (2014).
597 23. Turner, C. T., Lim, D. & Granville, D. J. Granzyme B in skin inflammation and disease.
598 *Matrix Biol.* **75–76**, 126–140 (2019).
599 24. Buzza, M. S. *et al.* Extracellular Matrix Remodeling by Human Granzyme B via Cleavage of
600 Vitronectin, Fibronectin, and Laminin. *J. Biol. Chem.* **280**, 23549–23558 (2005).
601 25. Champagne, D. E. Antihemostatic Molecules from Saliva of Blood-Feeding Arthropods.
602 *Pathophysiol. Haemost. Thromb.* **34**, 221–227 (2005).
603 26. Lefteri, D. A. *et al. Mosquito saliva sialokinin-dependent enhancement of arbovirus*
604 *infection through endothelial barrier leakage*.
605 http://biorxiv.org/lookup/doi/10.1101/2021.02.19.431961 (2021)
606 doi:10.1101/2021.02.19.431961.
607 27. Bardina, S. V. *et al.* Differential Roles of Chemokines CCL2 and CCL7 in Monocytosis and
608 Leukocyte Migration during West Nile Virus Infection. *J. Immunol.* **195**, 4306–4318 (2015).
609 28. Mills, C. D. Anatomy of a Discovery: M1 and M2 Macrophages. *Front. Immunol.* **6**, (2015).
610 29. Lamana, A. *et al.* CD69 Modulates Sphingosine-1-Phosphate-Induced Migration of Skin
611 Dendritic Cells. *J. Invest. Dermatol.* **131**, 1503–1512 (2011).
612 30. Mackay, L. K. *et al.* Cutting Edge: CD69 Interference with Sphingosine-1-Phosphate
613 Receptor Function Regulates Peripheral T Cell Retention. *J. Immunol.* **194**, 2059–2063
614 (2015).
615 31. Rajarathnam, K., Schnoor, M., Richardson, R. M. & Rajagopal, S. How do chemokines
616 navigate neutrophils to the target site: Dissecting the structural mechanisms and signaling
617 pathways. *Cell. Signal.* **54**, 69–80 (2019).

618 32. Pingen, M. *et al.* Host Inflammatory Response to Mosquito Bites Enhances the Severity of
619 Arbovirus Infection. *Immunity* **44**, 1455–1469 (2016).
620 33. Dey, R. *et al.* Gut Microbes Egested during Bites of Infected Sand Flies Augment Severity of
621 Leishmaniasis via Inflammasome-Derived IL-1β. *Cell Host Microbe* **23**, 134-143.e6 (2018).
622 34. Gough, P., Ganesan, S. & Datta, S. K. IL-20 Signaling in Activated Human Neutrophils
623 Inhibits Neutrophil Migration and Function. *J. Immunol.* **198**, 4373–4382 (2017).
624 35. Myles, I. A. *et al.* Signaling via the IL-20 receptor inhibits cutaneous production of IL-1β
625 and IL-17A to promote infection with methicillin-resistant Staphylococcus aureus. *Nat.*
626 *Immunol.* **14**, 804–811 (2013).
627 36. Shimizu, K. *et al.* PD-1 Imposes Qualitative Control of Cellular Transcriptomes in Response
628 to T Cell Activation. *Mol. Cell* **77**, 937-950.e6 (2020).
629 37. Wei, F. *et al.* Strength of PD-1 signaling differentially affects T-cell effector functions. *Proc.*
630 *Natl. Acad. Sci.* **110**, E2480–E2489 (2013).
631 38. Duyen, H. T. L. *et al.* Skin dendritic cell and T cell activation associated with dengue shock
632 syndrome. *Sci. Rep.* **7**, 14224 (2017).
633 39. Mommert, S., Schaper, J. T., Schaper-Gerhardt, K., Gutzmer, R. & Werfel, T. Histamine
634 Increases Th2 Cytokine-Induced CCL18 Expression in Human M2 Macrophages. *Int. J. Mol.*
635 *Sci.* **22**, 11648 (2021).
636 40. Chiffoleau, E. C-Type Lectin-Like Receptors As Emerging Orchestrators of Sterile
637 Inflammation Represent Potential Therapeutic Targets. *Front. Immunol.* **9**, 227 (2018).
638 41. Holmskov, U., Thiel, S. & Jensenius, J. C. Collectins and Ficolins: Humoral Lectins of the
639 Innate Immune Defense. *Annu. Rev. Immunol.* **21**, 547–578 (2003).

640 42. Tang, L. *et al.* Liver Sinusoidal Endothelial Cell Lectin, LSECtin, NegativelyRegulates
641 Hepatic T-Cell Immune Response. *Gastroenterology* **137**, 1498-1508.e5 (2009).
642 43. Kuo, P. T. *et al.* The Role of CXCR3 and Its Chemokine Ligands in Skin Disease and
643 Cancer. *Front. Med.* **5**, 271 (2018).
644 44. Niyonsaba, F., Ogawa, H. & Nagaoka, I. Human beta-defensin-2 functions as a chemotactic
645 agent for tumour necrosis factor-alpha-treated human neutrophils. *Immunology* **111**, 273–281
646 (2004).
647 45. Niyonsaba, F., Iwabuchi, K., Matsuda, H., Ogawa, H. & Nagaoka, I. Epithelial cell-derived
648 human β-defensin-2 acts as a chemotaxin for mast cells through a pertussis toxin-sensitive
649 and phospholipase C-dependent pathway. *Int. Immunol.* **14**, 421–426 (2002).
650 46. Rizzo, C. *et al.* IgG1 and IgG4 Antibody Responses to the Anopheles gambiae Salivary
651 Protein gSG6 in the Sympatric Ethnic Groups Mossi and Fulani in a Malaria Hyperhendemic
652 Area of Burkina Faso. *PLoS ONE* **9**, e96130 (2014).
653 47. Manning, J. E. *et al.* Safety and immunogenicity of a mosquito saliva peptide-based vaccine:
654 a randomised, placebo-controlled, double-blind, phase 1 trial. *The Lancet*
655 S0140673620310485 (2020) doi:10.1016/S0140-6736(20)31048-5.
656 48. Oliveira, F. *et al.* A sand fly salivary protein vaccine shows efficacy against vector-
657 transmitted cutaneous leishmaniasis in nonhuman primates. *Sci. Transl. Med.* **7**, (2015).
658 49. Sajid, A. *et al.* mRNA vaccination induces tick resistance and prevents transmission of the
659 Lyme disease agent. *Sci. Transl. Med.* **13**, eabj9827 (2021).
660 50. Bryden, S. R. *et al.* Pan-viral protection against arboviruses by activating skin macrophages
661 at the inoculation site. *Sci. Transl. Med.* **12**, eaax2421 (2020).

662 51. Bolger, A. M., Lohse, M. & Usadel, B. Trimmomatic: a flexible trimmer for Illumina
663 sequence data. *Bioinformatics* **30**, 2114–2120 (2014).
664 52. Li, B. & Dewey, C. N. RSEM: accurate transcript quantification from RNA-Seq data with or
665 without a reference genome. *BMC Bioinformatics* **12**, 323 (2011).
666 53. Langmead, B. & Salzberg, S. L. Fast gapped-read alignment with Bowtie 2. *Nat. Methods* **9**,
667 357–359 (2012).
668 54. Dobin, A. & Gingeras, T. R. Mapping RNA-seq Reads with STAR. *Curr. Protoc.*
669 *Bioinforma.* **51**, (2015).
670 55. Love, M. I., Huber, W. & Anders, S. Moderated estimation of fold change and dispersion for
671 RNA-seq data with DESeq2. *Genome Biol.* **15**, 550 (2014).
672 56. Huber, W., von Heydebreck, A., Sultmann, H., Poustka, A. & Vingron, M. Variance
673 stabilization applied to microarray data calibration and to the quantification of differential
674 expression. *Bioinformatics* **18**, S96–S104 (2002).
675 57. Zhu, A., Ibrahim, J. G. & Love, M. I. Heavy-tailed prior distributions for sequence count
676 data: removing the noise and preserving large differences. *Bioinformatics* **35**, 2084–2092
677 (2019).
678 58. Benjamini, Y. & Hochberg, Y. Controlling the False Discovery Rate: A Practical and
679 Powerful Approach to Multiple Testing. *J. R. Stat. Soc. Ser. B Methodol.* **57**, 289–300
680 (1995).
681 59. Blighe, K., Rana, S. & Lewis, M. Enhanced Volcano: publication-ready volcano plots with
682 enhanced colouring and labeling. (2021).
683 60. Walter, W., Sánchez-Cabo, F. & Ricote, M. GOplot: an R package for visually combining
684 expression data with functional analysis: Fig. 1. *Bioinformatics* **31**, 2912–2914 (2015).

685 61. Yu, G., Wang, L.-G., Han, Y. & He, Q.-Y. clusterProfiler: an R Package for Comparing
686 Biological Themes Among Gene Clusters. *OMICS J. Integr. Biol.* **16**, 284–287 (2012).
687 62. Yu, G. & He, Q.-Y. ReactomePA: an R/Bioconductor package for reactome pathway
688 analysis and visualization. *Mol. Biosyst.* **12**, 477–479 (2016).
689 63. Kolde, R. Pretty Heatmaps. R package version.
690 64. Sakai, R., Winand, R., Verbeiren, T., Moere, A. V. & Aerts, J. dendsort: modular leaf
691 ordering methods for dendrogram representations in R. *F1000Research* **3**, 177 (2014).
692 65. R Core Team (2021). *R: A language and environment for statistical computing. R*
693 *Foundation fo Statistical Computing, Vienna, Austria*. (The R Foundation).
694